Naval Research Laboratory
Washington, DC 20375-5320

NRL/6350/FR--2021/2

Realizing Novel Multifunctional Piezoelectrics for Next-Generation Sonar and Sensors

LAUREN GARTEN

Multifunctional Materials 6351
Material Science and Technology Division

July 27, 2021

REPORT DOCUMENTATION PAGE

Form Approved
OMB No. 0704-0188

1. REPORT DATE *(DD-MM-YYYY)*	**2. REPORT TYPE**	**3. DATES COVERED** *(From - To)*
27/03/2021	Karles Fellowship Report	October 2019- October 2020

4. TITLE AND SUBTITLE

Realizing Novel Multifunctional Piezoelectrics for Next-Generation Sonar and Sensors

5a. CONTRACT NUMBER

5b. GRANT NUMBER

5c. PROGRAM ELEMENT NUMBER
NISE

6. AUTHOR(S)

Lauren Garten

5d. PROJECT NUMBER

5e. TASK NUMBER

5f. WORK UNIT NUMBER
63-N2V7-00

7. PERFORMING ORGANIZATION NAME(S) AND ADDRESS(ES)

Naval Research Laboratory
4555 Overlook Avenue, SW
Washington, DC 20375-5320

8. PERFORMING ORGANIZATION REPORT NUMBER

NRL/6350/FR--2021/2

9. SPONSORING / MONITORING AGENCY NAME(S) AND ADDRESS(ES)

Naval Research Laboratory
4555 Overlook Avenue, SW
Washington, DC 20375-5320

10. SPONSOR/MONITOR'S ACRONYM(S)
NRL-NISE

11. SPONSOR/MONITOR'S REPORT NUMBER(S)

12. DISTRIBUTION / AVAILABILITY STATEMENT

DISTRIBUTION STATEMENT A: Approved for public release; distribution is unlimited.

13. SUPPLEMENTARY NOTES

Karles Fellowship

14. ABSTRACT

This report details the work performed by Lauren Garten during her Karles Fellowship. The research focused on the processing and characterization of lead-free piezoelectric materials for sensing and sonar applications. A processing route was established for the stabilization of $BaNiO_3$ ceramic powder and single crystals. Additionally a processing route was established to grow SnSe thin films by molecular beam epitaxy.

15. SUBJECT TERMS

Lead-free piezoelectrics, ceramic processing

16. SECURITY CLASSIFICATION OF:			**17. LIMITATION OF ABSTRACT**	**18. NUMBER OF PAGES**	**19a. NAME OF RESPONSIBLE PERSON**
a. REPORT	**b. ABSTRACT**	**c. THIS PAGE**			Lauren Garten
U/U	U/U	U/U	SAR	27	**19b. TELEPHONE NUMBER** *(include area code)* 202-767-1278

This page intentionally left blank

CONTENTS

This page intentionally left blank

EXECUTIVE SUMMARY

Piezoelectric materials enable many critical Navy technologies such as sonar, sensors, medical ultrasound, electronics, resonators, actuators and energy harvesters. Two new materials were identified that could exhibit a piezoelectric response greater than the materials currently deployed in many Navy sonar transducers (such as $Pb(Zr,Ti)O_3$ (PZT)). These materials are the $P6_3cm$ phase of $BaNiO_3$ (BNO) and the Pnma phase of SnSe at the monolayer limit. Developing growth processes for these complex bulk and 2D materials is the first step toward vetting the predictions of a large piezoelectric response in these materials. Processing methods were developed for the growth of two material systems. Barium nickelate powders were developed by solution processing, solid state reactions from nitrate and oxide precursors, and single crystal growth. The $BaNiO_3$ state was stabilized and the residual carbonates were reduced. Some lower-oxidation-state material was still present in these materials likely due to the limited activity of oxygen at the annealing temperature needed to reduce the carbonates. Still, the XRD results suggest that the BNO phase that was stabilized is in fact the non-centrosymmetric structure that is desired for piezoelectric measurements, the $P6_3cm$ phase. The second material system was SnSe. Thin films of SnSe were grown by molecular beam epitaxy. The composition of the films was found to be insensitive to the flux ratio between tin and selenium, but the flux ratios did impact the surface roughness and crystallographic orientation of the films. The deposition timing was determined in order to capture the initial stages of growth near the monolayer limit. These results show the importance of the surface preparation of the substrate on the films' nucleation. Overall, a processing method was developed to create high quality, well oriented, stoichiometric, Pnma phase thin films of SnSe.

This page intentionally left blank

REALIZING NOVEL MULTIFUNCTIONAL PIEZOELECTRICS FOR NEXT-GENERATION SONAR AND SENSORS

PREFACE

This report details the work performed by Dr. Lauren M. Garten while supported by the Jerome and Isabella Karle Distinguished Scholar Fellowship at U.S. Naval Research Laboratory from October 2019 to October 2020. This research focused on the development of processing methods for piezoelectric materials.

1. INTRODUCTION

1.1 Piezoelectricity and Piezoelectric Materials

Piezoelectric materials enable many critical Navy technologies such as sonar, sensors, medical ultrasound, electronics, resonators, actuators and energy harvesters. [1–3] Piezoelectrics are so ubiquitous that advances in piezoelectric performance could be translated rapidly across many applications, providing many benefits to the war fighter. Piezoelectricity is defined as a linear strain response induced in a material by an electric field, or vice versa, a polarization induced by an applied stress. [4] Piezoelectricity occurs in materials that lack a center of symmetry, limiting the search for intrinsically piezoelectric materials to 20 crystallographic point groups. [5] Piezoelectricity is also a prerequisite for additional properties such as ferroelectricity and multiferroism, which adds additional applications and benefits. For a material to be ferroelectric it must exhibit a spontaneous electrical polarization that can be reoriented with an applied electric field. [6, 7] Unlike ferromagnetism, in which the magnetic moment is defined for a single atom, [8] the spontaneous ferroelectric polarization develops due to the difference in the centers of net negative and net positive charge within each unit cell. Thus, determining the crystal structure of a material is critical to understanding the piezoelectric, ferroelectric, or multiferroic response that that material could have.

While the applications for piezoelectricity are extensive, there are still many challenges to overcome when optimizing piezoelectric performance. For example, many (if not all) of the best-performing piezoelectric materials contain lead, which, given new limitations on the use of lead, could lead to limitations in the use or processing of these materials. [9] In addition to regulations that limit the use of common piezoelectric precursors, many of the constituent materials used in piezoelectrics, such as lead or alkalis, are not available in nanofabrication facilities, again limiting the development of piezoelectric technologies. But the largest challenge for the development of many piezoelectric applications is the simultaneous optimization of multiple properties. Our previous work has focused on searching through derivatives of known materials in order to optimize a single property of a piezoelectric material. However, achieving the full potential of these piezoelectric technologies requires optimizing multiple properties simultaneously (e.g., temperature stability, permittivity, bandgap, breakdown strength, etc.). High-performance, multifunctional piezoelectric materials are critical for next-generation low-power switches, sensors, and memory [10, 11]. The ability to establish a Pb-free, high-performance piezoelectric material from earth-abundant, nontoxic elements that can be integrated into existing MEMs devices addresses an important shortcoming of existing piezoelectric materials.

Manuscript approved July 27, 2021.

1.2 The Search for New Bulk Piezoelectric Materials

The recent development of materials databases has allowed for the rapid multi-property search for new potential piezoelectric and ferroelectric materials. For example, previous work with the Materials Project (a Materials Genome-type material property database) team predicted a new piezoelectric phase of $SrHfO_3$. [12] Theory guided substrate epitaxy and beyond equilibrium deposition rates allowed us to realize the theoretically predicted piezoelectric P4*mm* phase of $SrHfO_3$, a high-energy polymorph, in competition with four other known structures. The piezoelectric response is consistent with the theory predictions, and the P4*mm* $SrHfO_3$ phase exhibits unique functionalities such as ferroelectricity.

Building upon this work, new materials were identified that could exhibit a piezoelectric response greater than that of the materials currently deployed in many Navy sonar transducers (such as $Pb(Zr,Ti)O_3$ (PZT)). One of these materials, the P6$_3$*cm* phase of $BaNiO_3$ (BNO), was selected as a candidate because of its large predicted piezoelectric coefficient. BNO is predicted to have a maximum e_{ij} piezoelectric coefficient of between 15 - 29 C/m^2, along with a predicted permittivity of 500. [REF: from the Materials Project Database based on reference [[13]] (https://materialsproject.org/materials/mp-19241/)] In turn, a higher piezoelectric coefficient allows for smaller, lighter devices such as point-of-use energy harvesters or electromechanical sensors.

Even though this material has been physically realized previously, there are many open questions about its structure and properties. The first reports of growth within the BNO material system in the literature were in 1971. [13] Still, there are conflicting reports on the point group of the ground state of BNO, with both P6/mmm and P6mm point groups being reported in literature. [14], [15] Determining the exact point group matters because only the non-centrosymmetric P6mm point group could be piezoelectric. It can be difficult to determine exactly what the ground state is when there are many polymorphs in competition but growth is not limited only to the most stable state, as many methods of stabilization could be considered similar to what has been done previously via strain, size, or atmosphere stabilization. [16]–[19]

If this compound does have the stoichiometry of $BaNiO_3$, then the nickel will be in a 4+ oxidation state, which is very rare. There is an open debate on the oxidation state of the nickel in this compound. [20] Because of the flexibility in the oxidation state of nickel, the BNO can be cycled through multiple oxidation states repeatedly. Recently, this cycling was observed and the solid solution relationship between $BaNiO_2$ and $BaNiO_3$ was determined. [21] This variability and recovery suggest this material could be used as an oxygen evolution reaction catalyst. [22] This oxygen-induced change in d-band filling also could change the character of the electrical, optical, and magnetic properties of the material. Additionally, band gap predictions for this material range from 1.55 eV to 8.9 eV. [14] If the band gap is large, then there is the potential for lower leakage currents and higher electric field operations. Dielectric measurements and impedance spectroscopy will be critical to the process iteration on the route toward a fully Ni 4+ state. These dielectric measurements leverage the author's previous experience in developing and adapting characterization techniques for complex piezoelectric materials. [23–25] If the materials are found to be insulating and piezoelectric, then there is also the possibility that these materials could be ferroelectric. There is a precedent for finding ferroelectricity and multiferroicity in similar materials with hexagonal crystal structures. [26] The first step toward vetting the theory predictions of the properties, particularly the piezoelectric response in this material, is to determine the crystal structure and composition.

1.3 The Search for 2D Piezoelectric Materials

Monolayer (Sn,Ge)Se thin films are predicted to have a higher piezoelectric coefficient than any currently known 2D material. The piezoelectric coefficients even are predicted to rival some commonly

used low-loss, lead-free, 3D piezoelectrics [27, 28]. A comparison of these predictions to the piezoelectric responses of some 2D materials (and other low-loss bulk piezoelectrics, such as AlN), shown in Fig. 1, underscores the transformative potential and scientific impact of these 2D monochalcogenide piezoelectrics. In particular, since these materials have strongly anisotropic bonding geometry, they can be transferred easily, and thus combined with other material systems, and easily integrated into flexible devices. Furthermore, as mentioned previously, materials that are piezoelectric also can be ferroelectric — where the spontaneous polarization can be reoriented in the presence of an electric field — and it has been proposed that these materials also should exhibit ferroelectricity. [29, 30] Realizing these unique 2D piezoelectric and ferroelectric materials open up unique future developments in flexible piezotronics, piezoelectric energy harvesters, and 2D ferroelectric memory. [31, 32] There is already significant interest in SnSe, GeSe, and (Sn,Ge)Se materials for solar cells, [33] flexible supercapacitors, [34] phase change materials, [35] lithium ion batteries, [36] and high-performance thermoelectric applications (ZT=2.6 at 923 K). [37] Developing these materials will allow us to study the cross coupling of functionalities between piezoelectricity and other properties that rarely occur in a single material.

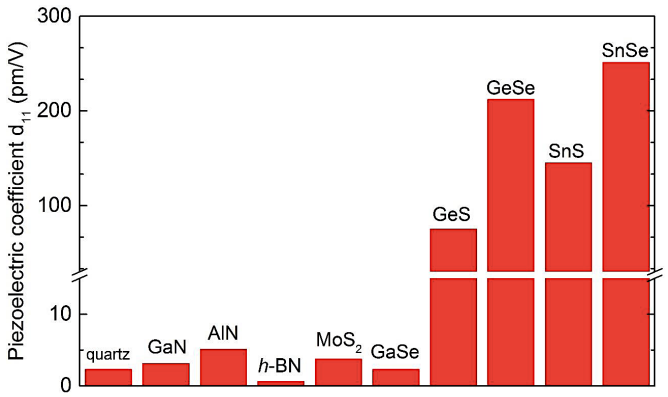

Fig. 1—A comparison of the piezoelectric coefficient d_{11} for 2D and 3D materials. The predicted response for SnSe and GeSe is significantly higher than those of other 2D materials such as MoS_2 and common piezoelectric thin film materials such as AlN. [38]

As piezoelectricity is dictated by symmetry, only films with odd layers will exhibit nonzero piezoelectric coefficients, and only a monolayer of these materials can exhibit the large piezoelectric response predicted. Because the ability to exfoliate these materials from bulk crystals has not yet been achieved, methods for the directional growth of these materials need to be developed in order to synthesize monolayers of these materials. The growth and characterization by molecular beam epitaxy would allow us not only to grow materials that we otherwise would not be able to access, but also to characterize structure and properties directly. Specifically, the molecular beam epitaxy capabilities will allow for the growth of the high-quality monolayer films directly, with the lateral dimension needed to test electrical properties and to evaluate electromechanical responses.

While a 2D material is unlikely to replace the piezoelectric single crystals currently used in sonar transducers, there are a number of unique advantages for 2D piezoelectrics. For example, reducing the dimensionality of the material while maintaining or even increasing the piezoelectric performance will reduce energy consumption and decrease waste heat. For electronic and piezoelectric applications in particular, reducing waste heat could lead to enhanced computation efficiency, and decreasing dimensions could reduce the weight and footprint of many sensors or energy harvesters.

1.4 Objective of This Work

The objective of this work is to develop processing routes to realize these selected bulk and two-dimensional materials with potentially high piezoelectric responses. First, the initial focus was on the synthesis and structural characterization of barium nickelate ($BaNiO_3$), and to use these materials to determine the crystal structure of the ground state, or most readily accessible state. A solution processing route was adapted from the literature for the development of BNO ceramic powder. [39] Solution processing was chosen because the high oxidation state of BNO likely prohibits other vacuum-based deposition techniques such as pulsed laser deposition, molecular beam epitaxy, or sputtering. Because of difficulties in acquiring the necessary chemicals for solution processing, other ceramic and crystal growth methods also were developed and tested. [40] The process of removing excess carbon from the precursor materials and achieving the necessary high oxidation state are discussed.

For the second portion of this work on 2D materials, the goal was to grow high-quality, monolayer films of SnSe with micrometer lateral dimensions. The growth was performed using an existing physical-vapor-deposition (PVD) system — Hybrid MBE (MBE 1), at the Pennsylvania State University under the guidance of Professor Roman Engel-Herbert's group. This MBE growth system allows for the thermal evaporation of high-purity Sn, Ge, and Se from conventional thermal effusion cells. The ultra-high vacuum environment (base pressure $1x10^{-10}$ Torr) and the use of very pure evaporation materials (semiconductor purity levels of 7N are commercially available for all three elements) facilitated the growth of high-quality monolayer material. Achieving wafer-scale SnSe films was done through a series of small systematic steps. Growth began on lattice matched substrates, such as MgO. Both in-situ and ex-situ feedback, such as reflective high-energy electron diffraction, X-ray diffraction, and atomic force microscopy, were used to iterate the growth parameters.

Developing growth processes for these complex bulk and 2D materials is the first step toward vetting the predictions of a large piezoelectric response in these materials. This work leverages previous experience in materials discovery, preliminary results on this material specifically, and an expertise in piezoelectric metrology development and characterization.

2. TECHNICAL APPROACH

2.1 Solution Processing of Barium Nickelate Powders

A solution growth method was developed based on an adaptation from the literature. [39] This method has the benefit of being achievable at low temperatures and under atmospheric conditions. Ethylenediamine is used as the chelating agent, which, in combination with nitric acid, forms ethylenediamine dinitrate, which blocks the precipitation of other alkaline earth nitrates and acts as a cross-linking agent. Nickel organic chelates also have been shown to stabilize nickel in the 4+ state. [39] The processing steps for this solution method were as follows:

1. Add precursors to 150 mL DI water and stir until dissolved
   - $Ba(NO_3)_2$ ---------- 0.789 g
   - $Ni(NO_3)_2$-$6H_2O$ --- 0.842 g
2. Add nitric acid ---------- 9 mL
3. Heat to 70°C, while stirring <Ramp: 20 mins, Hold: 30 mins>
4. Add additional acid
   - Citric acid ---------- 12 g
   - Ethylene glycol ------ 12 g
5. Stir <60 mins, @ 70°C>
6. Add ethylenediamine → pH = 10 [Added dropwise]

In the final step, the ethylenediamine was added dropwise while the pH was tested periodically with basic litmus paper. Large variations in the pH are possible due to the limited accuracy of color indicators. During the addition of the chelating agent, the solution went from green to purple or black. The next step was to determine the conditions for pyrolysis and calcination. Differential thermal analysis typically is used to look for changes during heat treatments. In this case, DTA/DSC could not be used due to the large increase in volume of the powder upon heating, leading to errors in the weight values. Still, the large volume increase has been seen previously, and does suggest that there is a large surface area present, which would help in reaching the required oxidation state. Thus, a range of different temperatures had to be tested directly for both steps. Table 1 shows the different temperatures used. Box furnaces with non-controlled atmospheres were used for the initial annealing. For the final experimental growths, a tube furnace with a controlled partial pressure of oxygen was used. For the final annealing, ramp rates were fixed at 2.5°C/min up to a temperature of 400°C; this slow ramp rate was used in case there were any residual solvent or organic precursors. Then a ramp rate of 5°C/min was used to reach the final temperature. The sample was held at temperature for two hours and then was cooled at either 5°C/min or the natural rate of cooling allowed by the system.

The structure of the material was characterized by X-ray diffraction (XRD). A copper k-alpha XRD system was used for measurements. The peaks in XRD were compared to standard PDF cards taken from the ICDD and ICSD on barium-containing compounds to determine the types of phases that were present.

Table 1—Solution Drying and Annealing Temperature Trials

Run	Solution Drying	Annealing Treatment	Results
B0	-	-	Disassociated
B1	150°C (24 h)	900°C (2h)	$BaCO_3$
B2	200°C (24 h)	900°C (2h)	$BaCO_3$ + $BaNiO_x$
B2-2	200°C (24) + 400 C (2)	1050°C (2h)	$BaNiO_3$+ $BaNiO_{2.5}$
B3	70°C (8h) +…	-	-
B4	400°C (2)	1050°C (2h)	$BaNiO_3$+ $BaNiO_{2.5}$

2.2 Molecular Beam Epitaxy of SnSe

For the growth of monolayer tin selenide (SnSe) thin films, molecular beam epitaxy was employed. This work was conducted externally during a period of shutdown at the Pennsylvania State University within the 2DCC research center. The first step in the growth of stoichiometric SnSe was to determine the flux ratio necessary to grow a 1:1 film. To measure the flux of each component, each effusion cell was set at a fixed temperature, then the deposition rate for a single cell was measured with a crystal monitor. This was repeated at multiple temperatures so the temperature dependence of each cell could be determined and fit to an equation that could be used to estimate particular flux values. Because selenium is more volatile than tin, flux ratios from 1:1 to 1:5 were investigated. Table 2 shows the selenium temperature needed to achieve this range of flux ratios.

Table 2—Selenium Temperature, Flux Rates, and Ratios

Se Temp	Flux Estimate (power law)	Goal	Flux Ratio – 1Sn:x Se	Equation
124.5	3.81724E+13	3.86E+13	2.00	$y=9E-14x^{12.709}$
129	5.99414E+13	6.01E+13	3	$y=9E-14x^{12.709}$
131.6	7.93807E+13	7.72E+13	4	$y=9E-14x^{12.709}$
133.5	9.52212E+13	9.65E+13	5	$y=9E-14x^{12.709}$
127.8	5.47263E+13	5.46E+13	3	$y=9E-14x^{12.709}$
131	7.28859E+13	7.28E+13	4	$y=8E-14x^{12.734}$
133.5	9.26795E+13	9.28E+13	5	$y=8E-14x^{12.735}$

The full design of experiments included flux ratios, substrate temperature, and deposition rate. The flux ratios were tested first from 1:1 to 1:5 at a fixed temperature of 250°C. Once an optimal flux rate was determined, the temperature of the substrate was varied from 250°C – 300°C. There was also some necessary preliminary work on the annealing of the MgO substrates prior to deposition to determine what conditions lead to pristine surfaces for thin film deposition. And finally, the deposition rate was tested to determine whether the initial stages of growth could be captured more effectively, as the goal is to deposit only a monolayer.

3. EXPERIMENTS

3.1 Growth Results for Barium Nickelate (BNO)

After the production of the solution, drying and annealing steps were necessary to create powder with the correct stoichiometry. Initial work focused at relatively low temperatures of 150°C for drying and a 900°C anneal for phase formation, as was suggested in the literature. These temperatures lead to significant amounts of $BaCO_3$ due to the residual carbon left from the organic precursors. Slightly higher drying temperatures then were tested to remove more of the volatile organics and solvent prior to annealing. These powders still had a significant amount of residual carbonates. If that same powder then was treated to a two-stage annealing process at 400°C followed by a two-hour anneal at 1050°C, then the amount of excess carbonates was reduced below the detection limit of X-ray diffraction. The standards used for comparison of the various barium nickelate phases is shown below the XRD measurement in Fig. 2. The predominant phase was found to be $BaNiO_3$, although the exact polymorph was not clear. There was also the presence of another oxidation state of approximately $BaNiO_{2.5}$. A small amount of excess nickel also was present, which is consistent with an increased amount of nickel during batching in efforts to reduce the amount of barium carbonate. Finding other oxidation states of BNO is not surprising, especially given the increased temperature and fixed atmosphere of the box furnaces used during annealing. Other batching attempts after this second set of experiments were lost due to the quarantine restrictions.

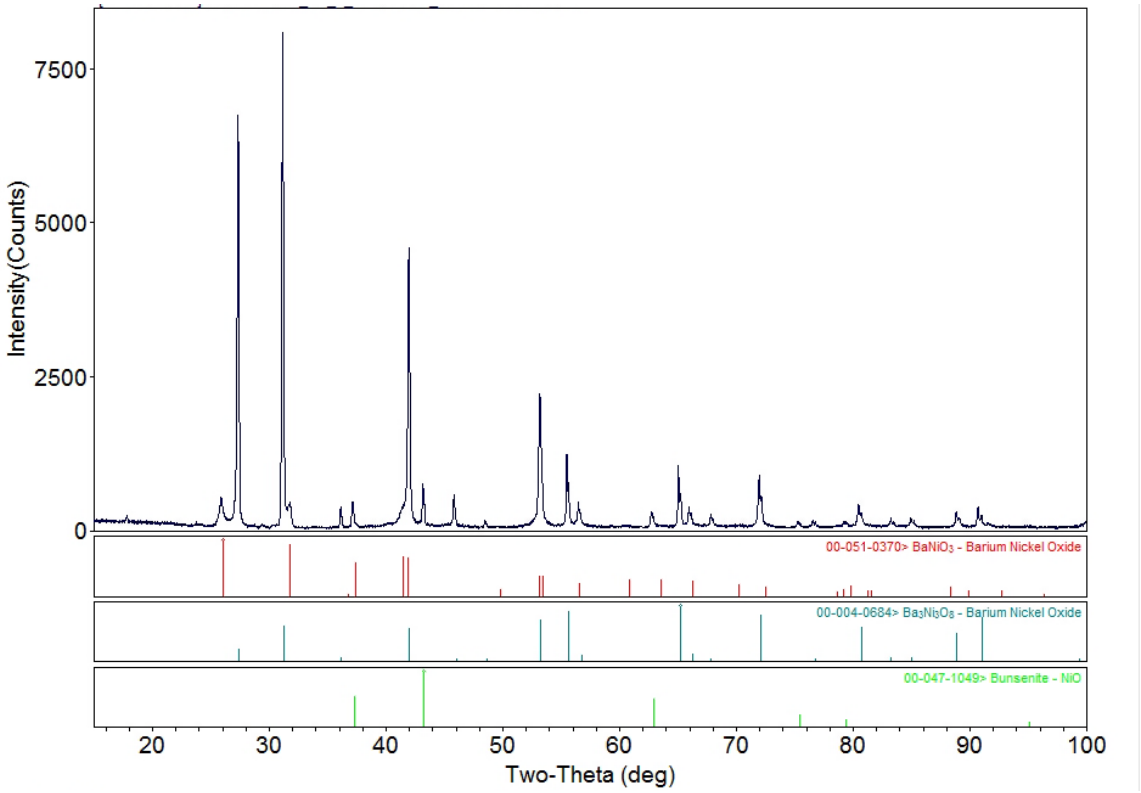

Fig. 2—X-ray diffraction results of BNO powder after a secondary anneal at 1050 °C to remove residual carbonates

Once the preponderance of the carbonates and second phases were removed, the next step was to try to increase the oxidation state of the nickel to reach stoichiometric $BaNiO_3$. To do this, powder from batch 4 annealed at 1050°C then was heat-treated again at lower temperature in constant flowing oxygen. Post annealing was done at temperatures of 600°C, 650°C, and 700°C. The XRD results for the powder processed at 600°C in constant flowing oxygen are shown in Fig. 3. While post annealing did increase the crystallinity of the samples, as indicated by the sharpening of the peaks, it did not reduce the presence of the secondary barium nickelate phase. Still, it is interesting to note that the peaks near 42° and 53° do show asymmetry consistent with what would be expected for the $P6_3cm$ phase (shown in the PDF card extracts below, where 01-072-0404 is the non-centrosymmetric $P6_3cm$ phase). Definitively determining the exact space group of the crystal structure would take more complex XRD analysis than what was available. Overall, the majority of the powder measured after annealing at 1050°C is in the $BaNiO_3$ phase.

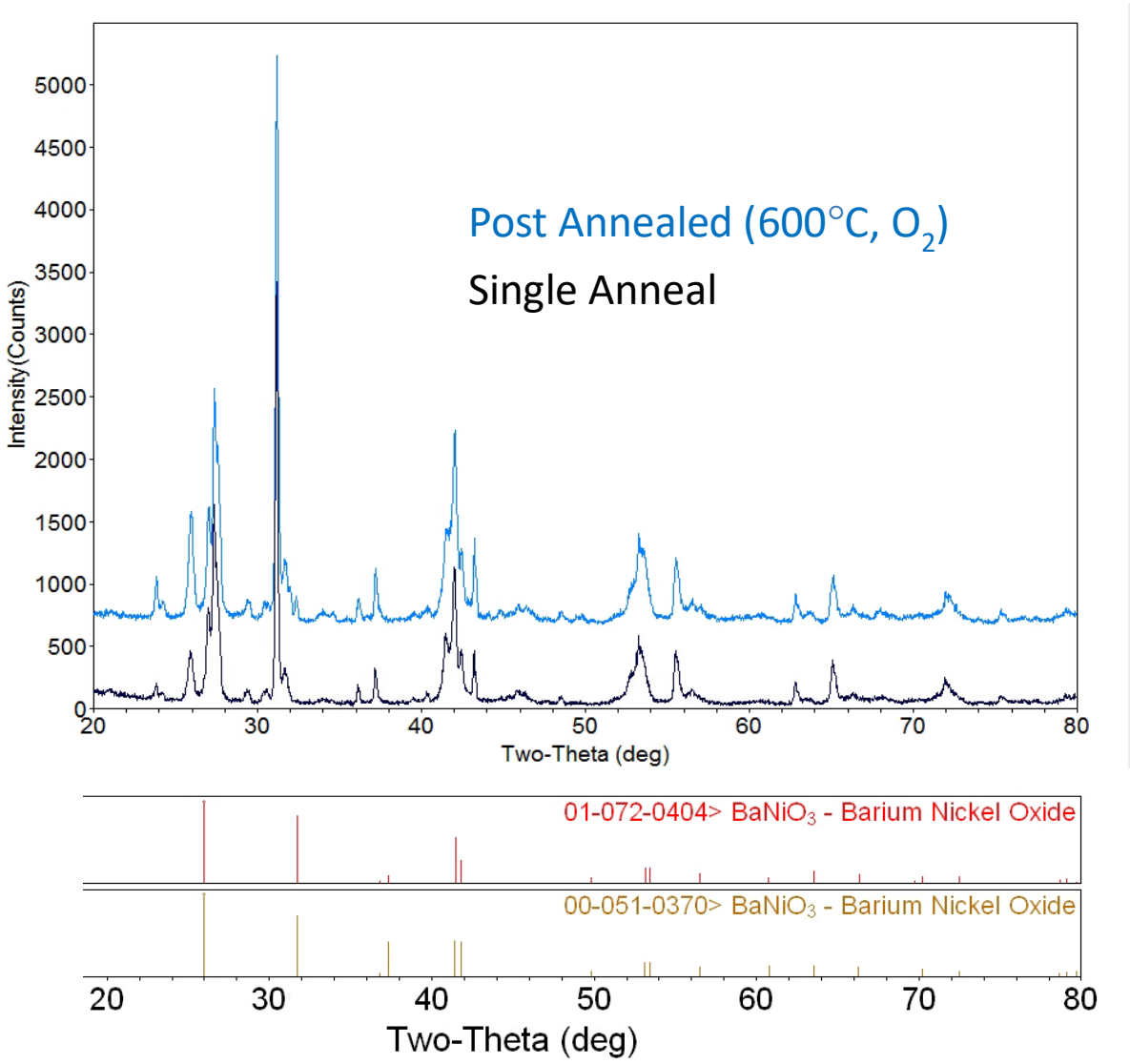

Fig. 3—X-ray diffraction results of BNO powder after a secondary anneal in flowing oxygen

Investigations also were made into the impact of the precursor materials on the formation of the Ni 4+ oxidation state in BNO. The first solid-state processing route used $BaCO_3$ and NiO as the starting precursors. The second employed barium nitrate and nickel nitrate as precursor materials. Figure 4 shows a comparison of the phase formation of the three different precursor materials. All materials were annealed under the same conditions at 1050°C for two hours. Each method did result in some portion of $BaNiO_3$ powder. The nitrate precursors exhibited excess nickel and residual nitrate byproducts. Surprisingly, the oxide-based precursors did not have an excess of residual carbonates, despite that being one of the constituent materials. Similar mixtures of oxidation states in the barium nickelate phase were found in all powders, regardless of the precursors used. However, the phase fraction of lower oxidation states did increase between sets of experiments, which could indicate absorption of water or degradation of precursor materials.

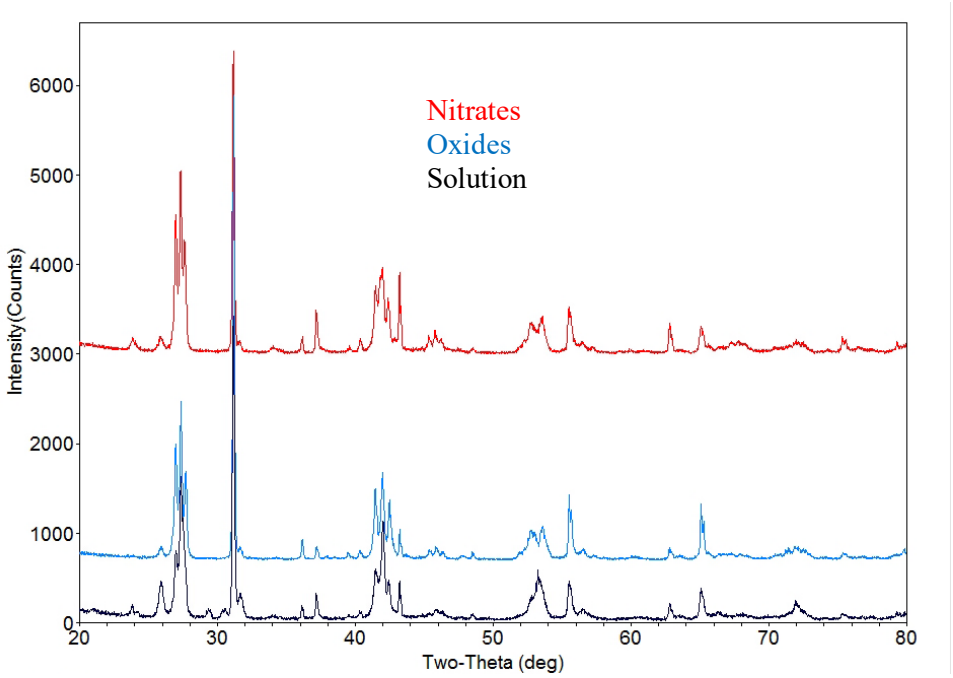

Fig. 4—X-ray diffraction results of BNO powder from nitrate, oxide, and solution-based precursors

The final growth attempt consisted of single-crystal growth of $BaNiO_3$. There are multiple reports in the literature on the growth methods for this crystal that were adapted for this study. [40] Precursor powder from the solid-state growth methods were used as the initial starting material for single-crystal growth. A flux of potassium hydroxide was used along with additional barium hydroxide. The powdered materials were mixed by mortar and pestle and then were placed into an alumina crucible. A tube furnace was used for the growths. A constant flow of oxygen was used to promote a higher oxidation state. The resulting materials formed elongated, black crystals approximately 0.5 mm in length. The crystal and flux solution were rinsed repeatedly until the KOH was visibly removed.

The results for this growth run are shown in Fig. 5. Barium nickelate is clearly present with strongly crystalline structure, consistent with the formation of large, single crystals that were observed after growth. The presence of barium carbonate at such a high percentage was unexpected. It is possible that the carbonates were left over from precursor $BaCO_3$ or had degraded into a carbonate during growth due to burnout from the furnace. The next step would be to grow single crystals using the solution-processed powders as the initial material. In this case, the materials needed to grow further solution powders were not available. Still the large crystalline growth and the strong crystallinity suggests that single crystal growth is a promising method for the growth of $BaNiO_3$ at a scale that would be needed for measurements.

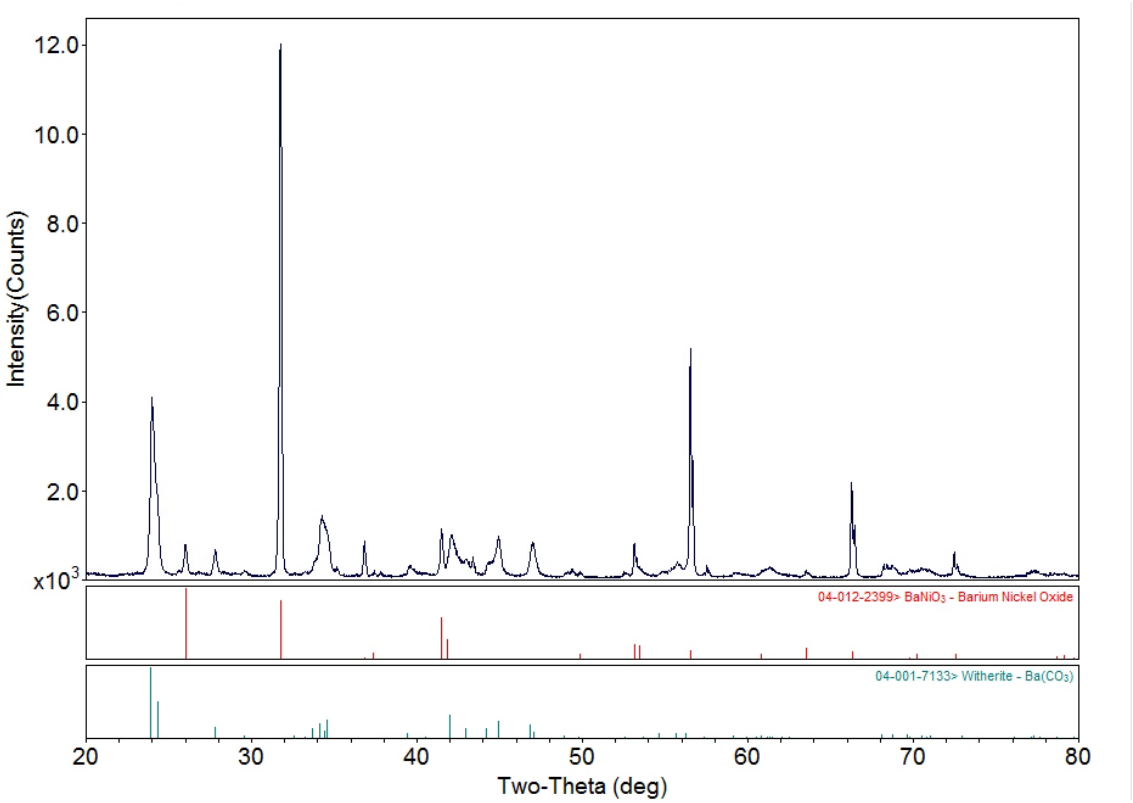

Fig. 5—X-ray diffraction results of BNO single crystals grown from a KOH flux

Overall, barium nickelate powders were grown from solution-based processing as well as solid-state and single-crystal reactions. The solution-based materials exhibit peak asymmetry consistent with a non-centrosymmetric material, such as the $P6_3cm$ phase. Post annealing in oxygen did not increase the phase fraction of a higher-oxidation-state material, suggesting that either more reactive oxygen or different annealing conditions are necessary to stabilize nickel in the 4+ state. This is counter to what has been seen previously in the literature, which could indicate high levels of process sensitivity to either the quality of initial materials, or the pyrolysis or annealing temperatures.

3.2 Growth Results for Tin Seleide (SnSe)

Thin films of tin selenide (SnSe) were grown by molecular beam epitaxy. The first step is to determine the flux rates and ratios as described in the approach section. The impact of the flux ratio on the stoichiometry, phase formation, and surface roughness were determined. For films grown with a flux ratio of 1:1 or 1:2, SnSe did not form. Instead the most likely phase to have formed was $SnSe_2$. For films with higher flux ratios, then SnSe did form. Figure 6 shows a comparison of the XRD results for film deposited at flux ratios of 1:4 (red), 1:4.5 (black), and 1:5 (blue) on MgO substrates at a temperature of 275 °C. Only the (2h 0 0) family of peaks appeared, indicating that the films are textured out of plane along the a-axis. The texturing weakened at the highest flux ratio, with secondary peaks beginning to emerge. The sharpest and highest peaks were for the 1:4.5 flux ratios, suggesting that these films had the highest quality. No other phases were observed in this flux range.

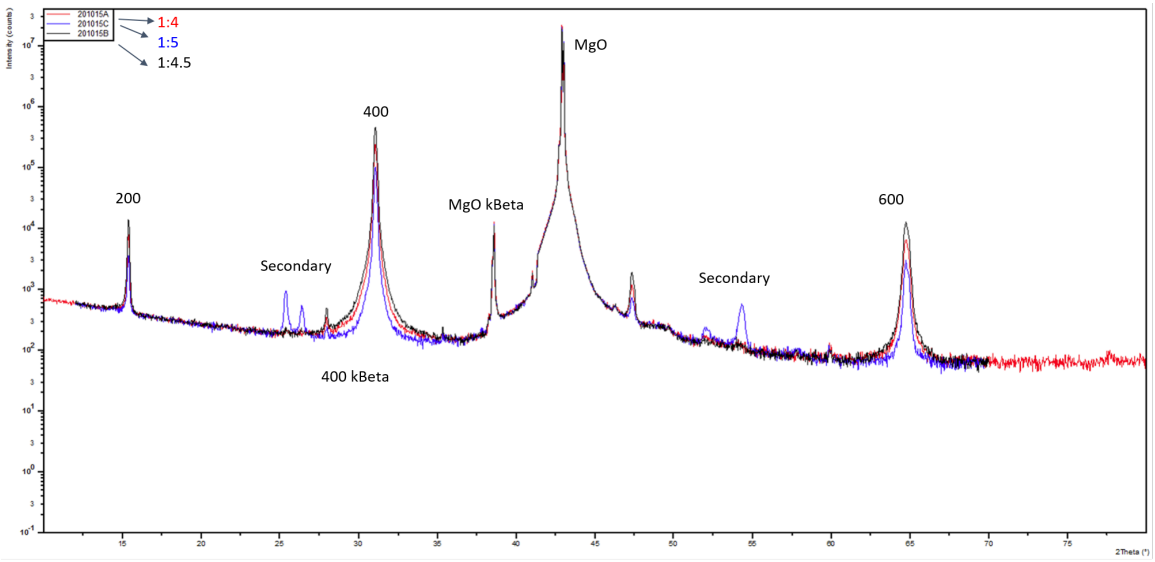

Fig. 6—X-ray diffraction results of SnSe thin films grown with different flux ratios

Once the crystal structure was determined, the next step was to verify the stoichiometry. X-ray photoelectron spectroscopy (XPS) was used to determine the composition and special variation by component in the thin films. Figure 7 shows the XPS results for a thin film of SnSe grown at a flux ratio of 1:5 at 275 °C. Each of the constituents (Sn, Se, Mg, O) is fit and the depth profile is developed from the change in response as a function of energy. At the surface of the film (from 0 – 10 nm), there is

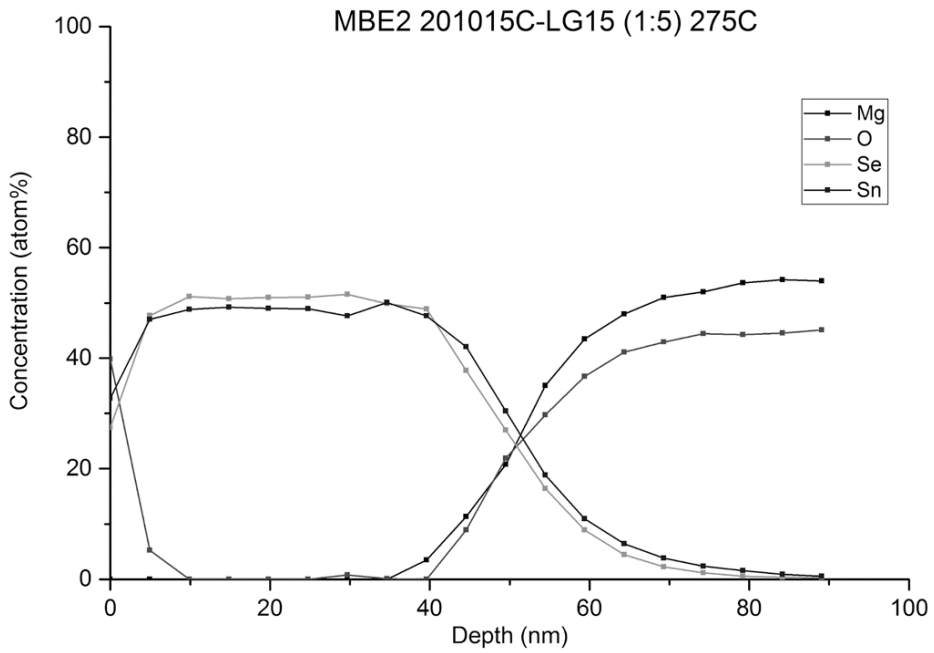

Figure 7. X-ray photoelectron spectroscopy results of SnSe thin films grown with a flux ratio of 1:5 at 275 C

a layer that contains a surface oxide, likely a tin oxide, due to reactions between the film and air. Within the thickness of the film (10 – 40 nm) the composition is approximately Sn:Se = 50:50. The films are approximately 50 nm thick. The same XPS analysis was run on samples across the flux ratio for films from 1:3 to 1:5 grown on both sapphire and MgO substrates.

Figure 8 shows a comparison of the composition of these samples as determined by XPS for the center of the film. All of the films that were grown with flux ratios from 1:3 to 1:5 showed within 5% of 1:1 stoichiometry. The composition of the films decreased slightly with increasing flux ratio, which was unexpected. Also, the flux ratio did not significantly impact the composition of the films, which differs from what was expected. Previous literature has shown that nearly stoichiometric SnSe could be deposited at flux ratios less than 1:1, which was not observed here. Part of the difference between what was expected and what was observed could be understood by looking at the deposition rates. Thin films of pure tin were deposited prior to any SnSe runs in order to determine the deposition rate and thus to get a second data point for the flux of Sn. When the deposition rate of the SnSe films was compared to that of pure tin films, it was found to be significantly slower than what would be expected from the deposition rates calculated for pure tin. This suggests that both selenium and SnSe are volatile because if the tin was depositing at the same rate as when selenium was not present, then the films should have been non-stoichiometric. Further work is necessary to determine the kinetics that occur during the deposition of the films.

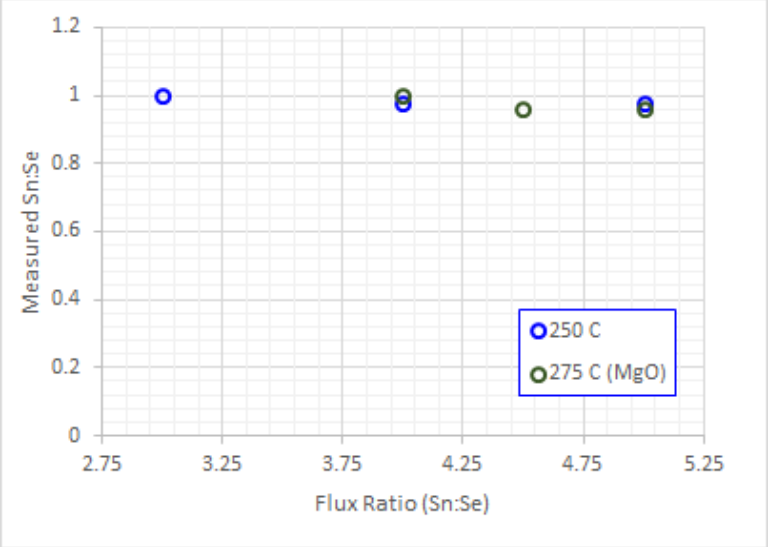

Fig. 8—Comparison of the x-ray photoelectron spectroscopy results of SnSe thin films as a function of flux ratio

Reflection high-energy electron diffraction (RHEED) is another useful tool to track the development of structure and composition during growth. Figure 9a shows the RHEED pattern taken on the MgO substrate prior to deposition. Figure 9b shows the RHEED pattern for a SnSe film grown at 275°C on MgO with a flux ratio of 1:4.5. The streaky patterns seen in the RHEED of the film indicate that there is a continuous crystalline structure in the plane of the film. The spacing is consistent with that expected for the Orthorhomic Pnma (62) phase of SnSe with a Van der Waals gap between the (100) planes. The expected lattice parameters for bulk and monolayer films are a(bulk) = 11.50 Å (2 ML), b(bulk) = 4.15 Å : b(ML) = 4.24 Å, c(bulk) = 4.44 Å : c(ML) = 4.35 Å. It is expected that the a-axis will be out of plane, given the fit between the b and c lattice to the MgO substrate. This is what is seen in all structural characterization. The RHEED results are consistent with the structure observed by XRD, indicating that

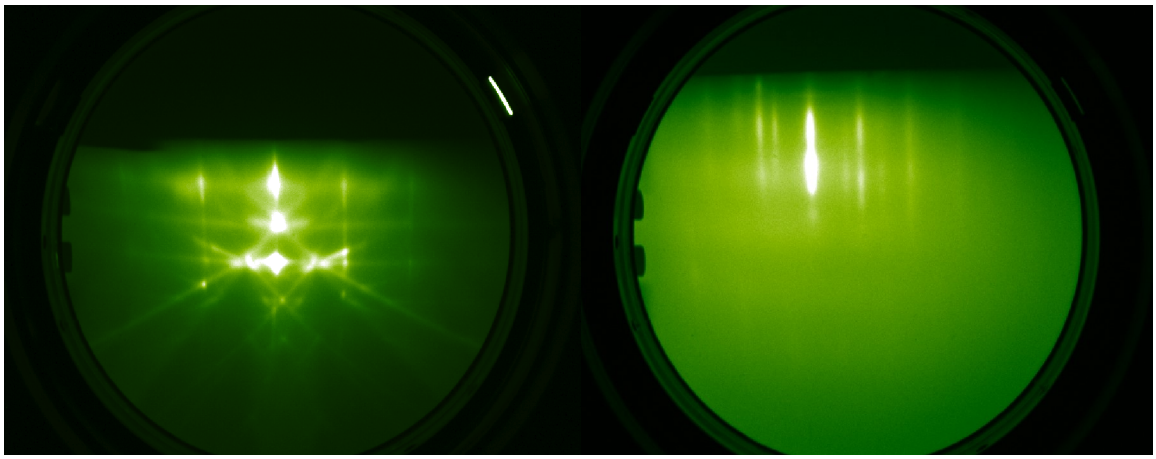

(a) (b)

Fig. 9—(a) The RHEED pattern taken on the MgO substrate prior to deposition. (b) shows the RHEED pattern for a SnSe film grown at 275 °C on MgO with a flux ratio of 1:4.5.

the correct phase of SnSe, the Pnma phase, was stabilized. In fact, if the XRD results from the thin films with a 1:4.5 ratio grown on MgO at 275°C are overlaid on those taken on a cleaved single crystal of SnSe, the films' peaks line up with those for the single crystal. This indicates that thin films with thickness of at least 50 nm exhibit lattice parameters that are closer to the bulk values than those toward the monolayer limit. Overall, the RHEED, XPS, and XRD results show that SnSe films with the correct stoichiometry were grown in the expected Pnma phase, with the desired a-axis orientation.

Figure 10 shows an overlay of the XRD results for a SnSe film grown at 275 °C on MgO with a flux ratio of 1:4.5 and cleaved single crystals of SnSe.

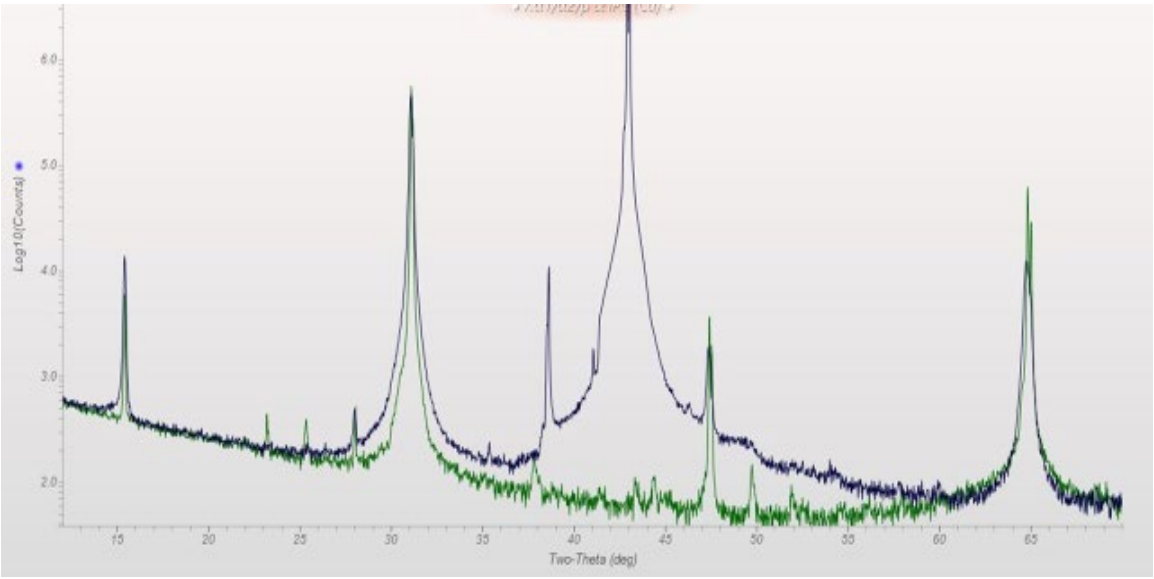

Fig. 10—An overlay of the XRD results for a SnSe film grown at 275 °C on MgO with a flux ratio of 1:4.5 and cleaved single crystals of SnSe

Another aspect that was influenced by the flux ratio is the surface roughness, which was measured using atomic force microscopy (AFM). Figure 11 shows a comparison between three different AFM images of the surface roughness of the films. Figure 11a shows AFM results for a film grown at 250°C at

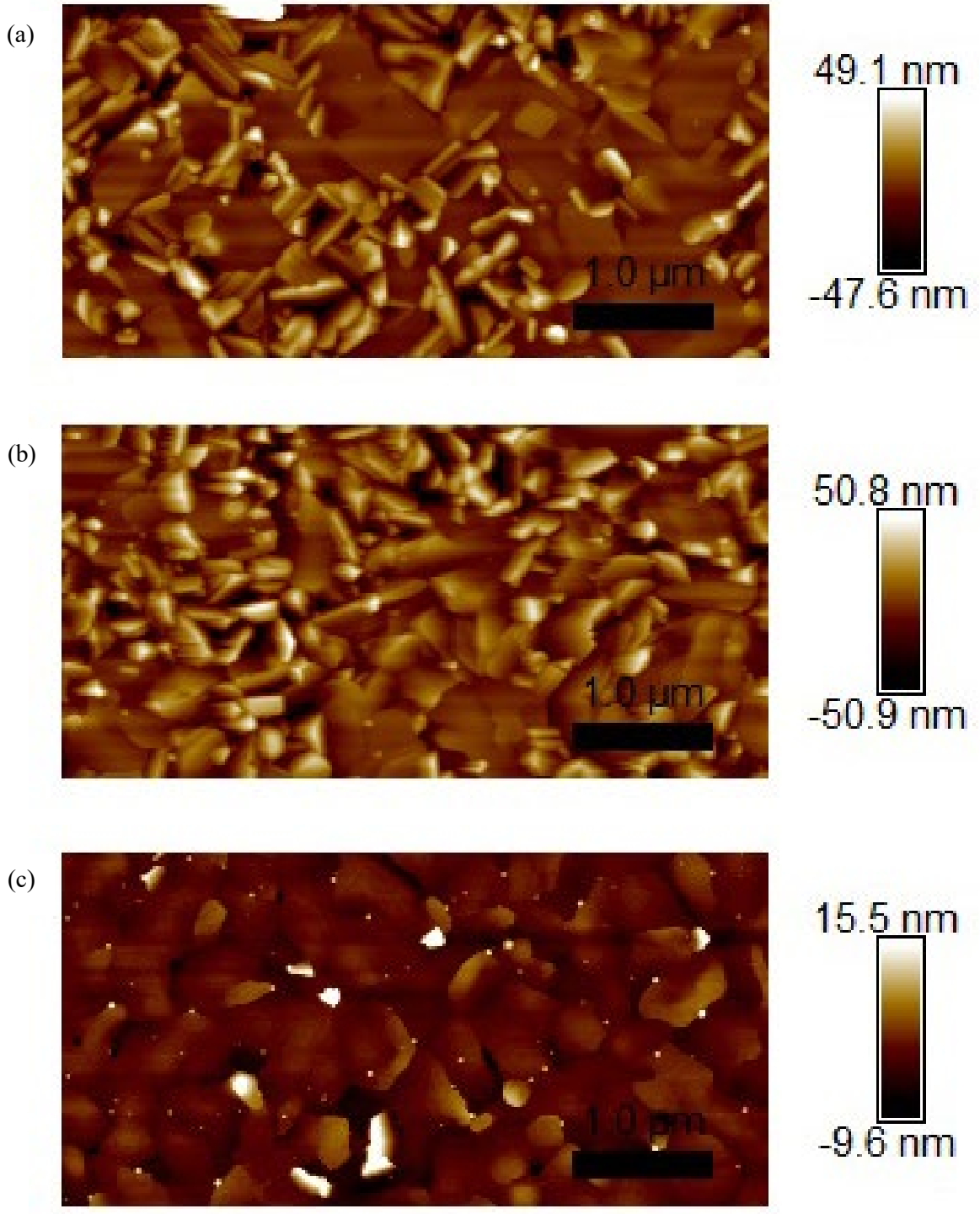

Fig. 11—AFM results for (a) a film grown at 250°C at a flux ratio of 1:4.5, (b) a film at 1:5 at 285°C,and (c) a film at 285°C at a flux ratio of 1:4.5.

a flux ratio of 1:4.5. The middle figure, Fig. 11b, shows the results for a film at 1:5 at 285°C, and Fig. 11c shows the AFM results of a film at 285°C at a flux ratio of 1:4.5. The rough surface for the films grown at lower temperatures is consistent with the XRD showing a distribution of different crystallographic orientations. These crystallites can be seen growing at an angle between the larger flat plates. Still, the preponderance of the films is a-axis-oriented and relatively flat. When films are grown at higher temperatures at a flux rate of 1:5, there is an increase in the surface roughness. This suggests that the nucleation of off-axis grains increases with increasing temperature. But if we look at the last figure grown at the same temperature with a lower flux rate the surface roughness decreases significantly. Thus the flux ratio has as great an impact as the temperature on the orientation of the films and thus the surface roughness.

As the goal is to measure the piezoelectric response of the films, it is necessary to minimize off-axis grains as much as possible so that a macroscopic symmetric breaking can be maintained. The hypothesis was that the higher flux led to a faster deposition, leaving the incoming atoms with little time to rearrange, so there was a higher potential for off-axis grains to form. It also would be expected that higher temperatures would give the atoms more mobility to move into the most energetically favorable orientation with the b- and c-axes in plane. To test this, the growth rate of the films was cut from 0.1 Å/sec to 0.025 Å/sec. Films were grown at a flux ratio of 1:4.5 at temperatures from 250 to 300°C.

Growing at slower speeds did not increase the quality of the films. The films had a much higher surface roughness, poorer crystallinity, and more misoriented grains. Figure 12 shows a RHEED pattern for a film grown at the slower rate at a flux ratio of 1:4.5. The polycrystalline pattern of the film is clear from the discretized spots in the RHEED pattern. The AFM for the same sample shows the origin of these polycrystalline diffraction spots comes from the fact that the majority of the film is off-axis grains with few a-axis grains interspersed. The structure of the grains with a triangular termination is a defining feature that is distinctly different from the flat a-axis-dominant films. The surface roughness increases significantly due to the presence of these smaller, deeper-grooved grains. Likewise, growing at slower rates and higher temperatures did not lead to significant changes in the surface roughness or crystalline quality up to 285°C. Beyond this, no films could be detected after deposition, indicating that the substrate temperature was hot enough to volatilize the SnSe. Growing at slower rates did not improve the surface quality of the films at any temperature or flux ratio, as would have been expected. This suggests that there is a more complex relationship between the growth conditions and the orientation of the nucleating films. In order to understand more about the initial stages of nucleation, the deposition experiments had to be redesigned to capture the initial stages of growth.

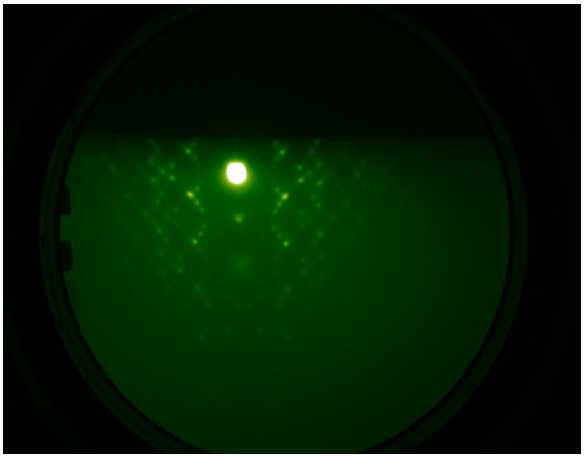

(a)

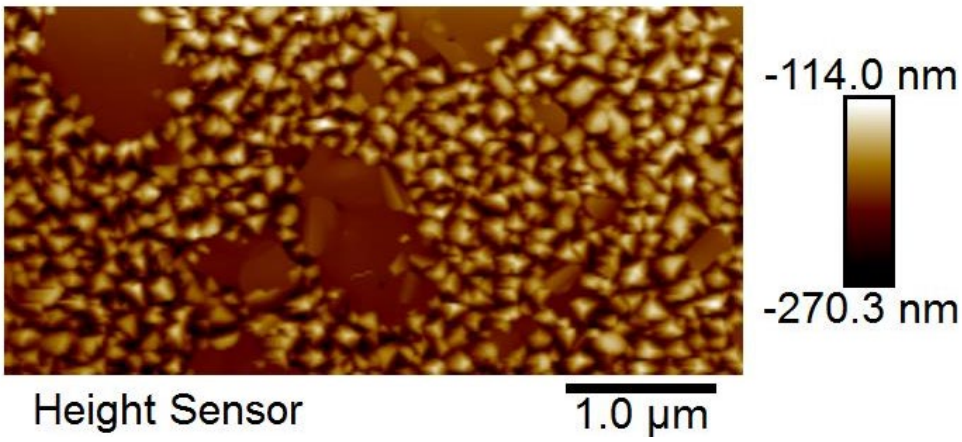

(b)

Fig. 12—(a) Shows the RHEED for a film grown at a slower rate with a flux ratio of 1:4.5. (b) Shows the results for an AFM scan of the same film grown at a slower rate.

In order to capture the initial stages of both, the growth and the characterization had to be revamped. The XPS data was used as a double check for the deposition rate of the films. Using these timing estimates, a program was developed to close the source shutters as soon as this time threshold was hit in order to capture the first few layers of growth. The faster growth rates were used and the substrate temperature was kept at 285°C, as this was found to be the best balance between achieving a high film orientation and the re-evaporation of the SnSe film. During these growths, the RHEED did not change in structure significantly; there was only a gradual dimming of the MgO streaks. This suggests that the films are not grown as a continuous film, because otherwise the MgO peaks would have diminished within a few layers. Again the growth rates were not consistent with the expected values from the "bulk" film growth. This again points to more complex kinetics occurring during the early stages of growth, where absorption and evaporation of the SnSe materials likely vary significantly. It is also likely that the film growth is extremely sensitive to the surface preparation of the MgO substrates. Variation between growth runs under the same conditions points toward the MgO termination playing a significant role in how the material sticks and what nuclei are formed during the early stages of growth. For a comparison, Fig. 13 shows the AFM results of a SnSe films grown under the conditions described above on a vacuum-annealed MgO substrate. The development of discrete nuclei is consistent with the observations made by RHEED. There are few smaller triangular grains that are likely the progenitors of the larger, grooved and

misoriented grains in the thicker films. Additionally it is interesting to note that the initial grains do not form with clear crystallographic orientation in-plane as is often seen in other 2D materials such as MoS_2. Instead, the in-plane orientation looks to be random, suggesting that the templating off of the MgO is not effective. The root mean square (rms) roughness of the samples is approximately 1.08 nm, with an average island height of 12 nm. Assuming an a-axis orientation, that would put these structures between the monolayer and bilayer thicknesses. This suggests that the method developed would be effective at capturing films at the monolayer limit for piezoelectric measurements.

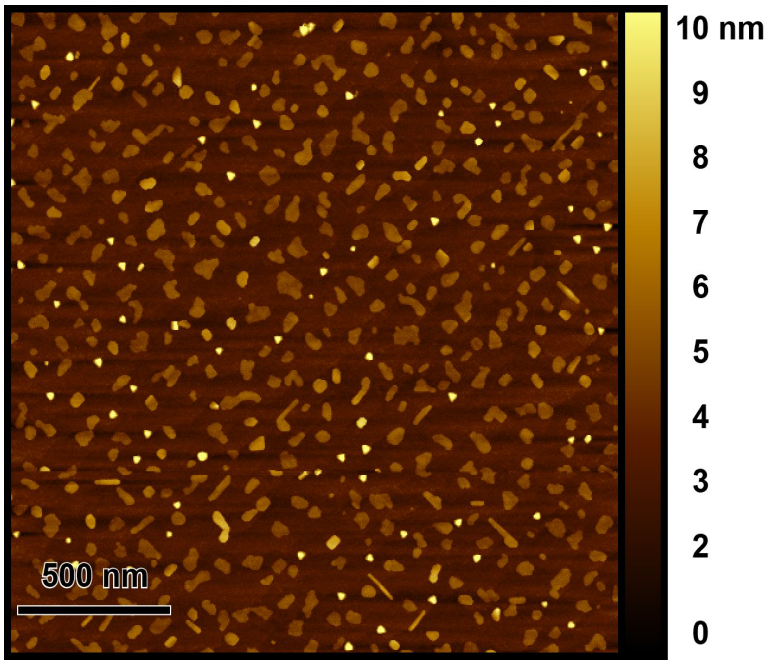

Fig. 13—AFM image of films grown on vacuum annealed MgO substrates near the monolayer limit

If we then compare the vacuum-annealed films to films grown under the same conditions but on substrates that were annealed under a low partial pressure of oxygen, there is a clear difference. Figure 14 shows the AFM results of a film grown on an oxygen-annealed substrate. There is a clear difference in the grain size as well as the grain structure. There are significantly more triangular grains even at a similar stage of growth. The in-plane-oriented grains are slightly large but fewer in number. The size of these grains would make it feasible to deposit electrodes using a direct write lithography approach for piezoelectric measurements. Again, these islands are near the monolayer limit. This suggests that more of the material has gone into nucleating misoriented grains. It could be expected from this data that as they grow thicker, these films will exhibit increased surface roughness and a broader distribution of grain orientations. Further study is needed to determine the entirety of the impact of surface preparation and termination on the MgO substrate on the growth of SnSe films, but these preliminary results point toward this being a critical factor in the film quality.

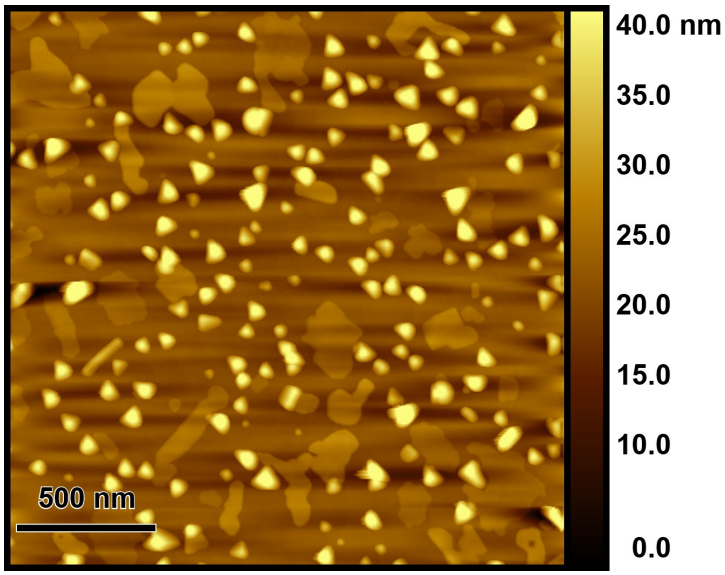

Fig. 14—AFM image of films grown on low-oxygen-annealed MgO substrates near the monolayer limit

In addition to changing the growth setup, the characterization tools needed to capture the structure during the first few layers of film growth also had to be adapted. XRD no longer could be used to determine the structure of the film due to the limited amount of material. Thus, Raman spectroscopy was used because it is more sensitive to smaller areas of material. Figure 15 shows an example of the Raman spectrum taken from a SnSe film grown at 285°C at a flux ratio of 1:4 with identification for the primary modes. All of the present modes fit for SnSe in the Pnma phase. There are no indications of any secondary phase, such as other polymorphs of SnSe, or different compositions of tin and selenium. These results also suggest that polarized Raman spectroscopy would be a useful tool for looking at the in-plane orientation, which will be critical for the piezoelectric measurements.

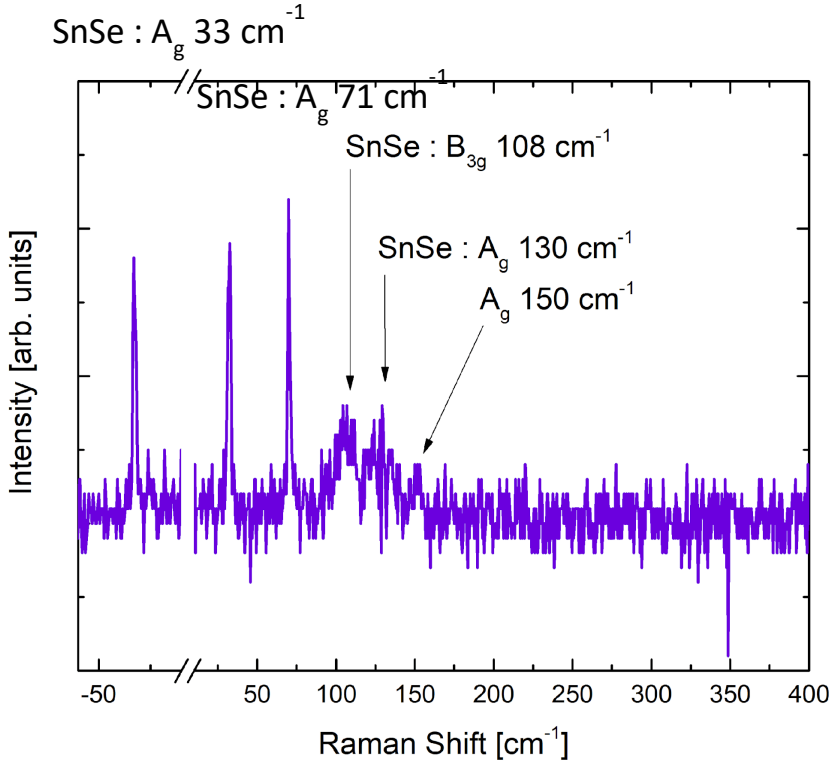

Fig. 15— Raman spectroscopy of a SnSe thin film growth at 285° C at a flux ratio of 1:4

Raman spectroscopy was used to look at the development of the structure during the initial stages of growth. Figure 16 shows the Raman spectra for film with decreasing film thickness (decreasing deposition time) with increasing y values. The black spectra is taken from a single crystal of SnSe for comparison. A Raman response is visible in all films that had a deposition time greater than 10 minutes. The structure seems to be consistent overall; however, there is some variation between samples grown under similar conditions, which likely traces back to the substrate preparation, as discussed in the previous section. There is a slight shift in the peaks' position with increasing thickness, which could point toward a change in strain or lattice parameters. Further work is necessary to determine how the crystal structure of SnSe changes upon approaching the monolayer limit. These results also show that the different grain structures are all the correct phase, leaving misorientation as the likely difference.

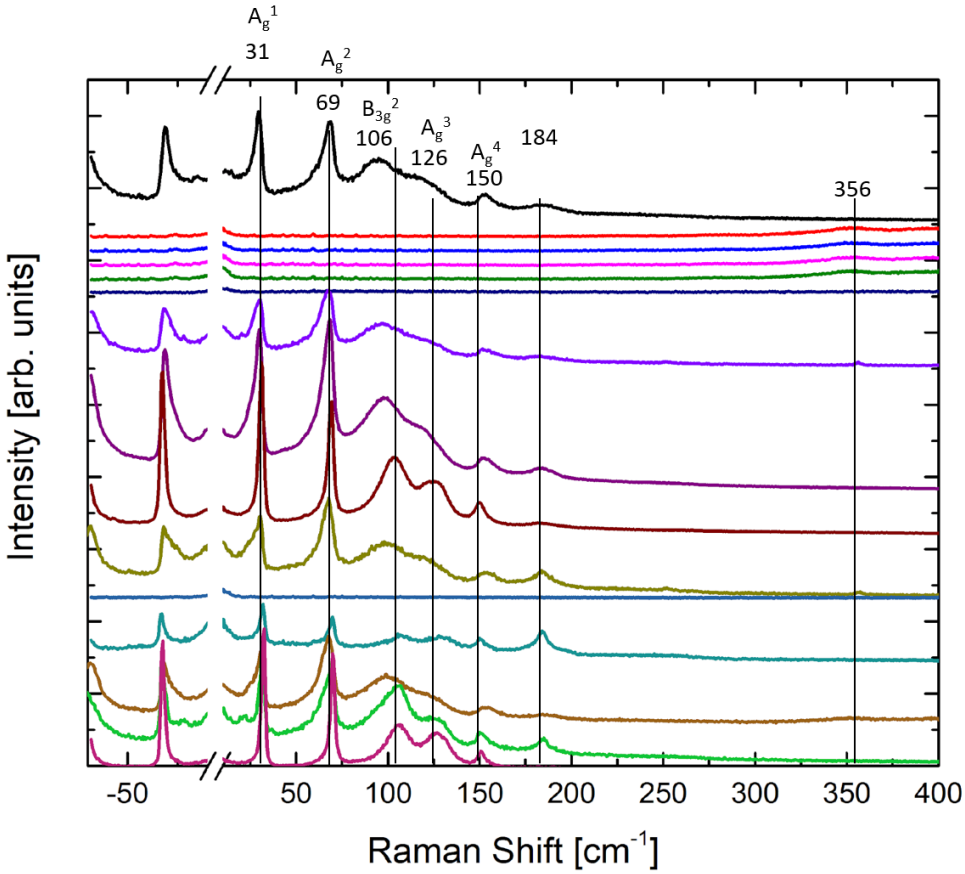

Fig. 16—Raman spectroscopy of SnSe thin films grown at 285°C as a function of time (increasing time with decreasing position), compared to a Raman spectra taken from a single crystal standard (black)

Overall, a processing method was developed for SnSe thin films. This process produces the correct phase, the Pnma structure, and the desired crystallographic orientation (a-axis). It was shown that the growth could be tailored to capture films near the monolayer limit, indicating that piezoelectric measurements are possible.

4. CONCLUSIONS

In conclusion, processing methods were developed for the growth of two material systems. Barium nickelate powders were developed by solution processing, solid state reactions from nitrate and oxide precursors, and single crystal growth. The $BaNiO_3$ state was stabilized and the residual carbonates were reduced. Some lower-oxidation-state material was still present in these materials, likely due to the limited activity of oxygen at the annealing temperature needed to reduce the carbonates. Still the XRD results suggest that the BNO phase that was stabilized is, in fact, the non-centrosymmetric structure that is desired for piezoelectric measurements, the $P6_3cm$ phase.

The second material system was SnSe. Thin films of SnSe were grown by molecular beam epitaxy. The composition of the films was found to be insensitive to the flux ratio between tin and selenium, but the flux ratios did impact the surface roughness and crystallographic orientation of the films. The deposition timing was determined in order to capture the initial stages of growth near the monolayer limit.

These results show the importance of the surface preparation of the substrate on the films' nucleation. Overall, a processing method was developed to create high-quality, well-oriented, stoichiometric, Pnma phase thin films of SnSe. The first stage in the development of potential piezoelectric materials is the characterization of their crystal structure.

REFERENCES

[1] Susan Trolier-McKinstry, "Ferroelectricity: A revolutionary century of discovery," pp. 22–30, 2020.

[2] L. Garten *et al.*, "Nonlinear dielectric response in piezoelectric materials for underwater transducers," *J. Appl. Phys.*, 2012.

[3] V. G. DeGiorgi, L. Garten, P. Finkel, and M. Staruch, "Transduction using functional materials: Basic science and understanding at the U.S. Naval Research Laboratory," in *ASME 2019 Conference on Smart Materials, Adaptive Structures and Intelligent Systems, SMASIS 2019*, 2019.

[4] B. Jaffe, *Ceramics Piezoelectric*. 1971.

[5] W. Cady, *Piezoelectricity: an introduction to the theory and applications of Electromechanical Phenomena in Crystals*. Dover Publications, 1964.

[6] M. E. Lines and A. M. Glass, *Principles and Applications of Ferroelectrics and Related Materials*. Oxford University Press, 2001.

[7] H. D. Megaw, "Origin of ferroelectricity in barium titanate and other perovskite-type crystals," *Acta Crystallogr.*, vol. 5, no. 6, pp. 739–749, Nov. 1952.

[8] R. M. Bozorth, *Ferromagnetism (Textbook)*. John Wiley & Sons, Inc., 2003.

[9] United States Enviromental Protection Agency, *The Frank R. Lautenberg Chemical Safety for the 21st Century Act*. 2016.

[10] P. Finkel, M. Staruch, A. Amin, M. Ahart, and S. E. Lofland, "Simultaneous Stress and Field Control of Sustainable Switching of Ferroelectric Phases," *Sci. Rep.*, vol. 5, no. 1, p. 13770, Nov. 2015.

[11] L. Baudry, I. Lukyanchuk, and V. M. Vinokur, "Ferroelectric symmetry-protected multibit memory cell," *Sci. Rep.*, vol. 7, no. 1, p. 42196, Dec. 2017.

[12] L. M. Garten *et al.*, "Theory-Guided Synthesis of a Metastable Lead-Free Piezoelectric Polymorph," *Adv. Mater.*, vol. 30, no. 25, Jun. 2018.

[13] H. Krischner, K. Torkar, and B. O. Kolbesen, "Beiträge zum system BaONiO," *J. Solid State Chem.*, vol. 3, no. 3, pp. 349–357, Aug. 1971.

[14] R. A. Evarestov, V. A. Veryazov, I. I. Tupitsyn, and V. V. Afanasiev, "The electronic structure of crystalline nickel oxides," *J. Electron Spectros. Relat. Phenomena*, vol. 68, no. C, pp. 555–563, May 1994.

[15] J. DiCarlo, I. Yazdi, A. J. Jacobson, and A. Navrotsky, "Preparation and thermochemical properties of BaNiO2+x," *J. Solid State Chem.*, vol. 109, no. 2, pp. 223–226, Apr. 1994.

[16] J. S. Mangum, L. M. Garten, V. Jacobson, D. S. Ginley, and B. P. Gorman, "Exploring the Link Between Amorphous Structure and Crystallization Behavior of Titania Thin Films by Electron-Based Pair Distribution Functions and in-situ TEM," *Microsc. Microanal.*, vol. 25, no. S2, pp. 1506–1507, Aug. 2019.

[17] J. S. Mangum, L. M. Garten, D. S. Ginley, and B. P. Gorman, "Utilizing TiO_2 amorphous precursors for polymorph selection: An in situ TEM study of phase formation and kinetics," *J. Am. Ceram. Soc.*, p. jace.16965, Dec. 2019.

[18] S. Siol *et al.*, "Negative-pressure polymorphs made by heterostructural alloying," *Sci. Adv.*, vol. 4, no. 4, 2018.

[19] B. R. Chen *et al.*, "Understanding crystallization pathways leading to manganese oxide polymorph formation," *Nat. Commun.*, vol. 9, no. 1, Dec. 2018.

[20] R. Gottschall, R. Schöllhorn, M. Muhler, N. Jansen, D. Walcher, and P. Gütlich, "Electronic State

of Nickel in Barium Nickel Oxide, BaNiO3," *Inorg. Chem.*, vol. 37, no. 7, pp. 1513–1518, 1998.
[21] A. M. Arévalo-López, M. Huvé, P. Simon, and O. Mentré, "The hidden story in BaNiO3 to BaNiO2 transformation: Adaptive structural series and NiO exsolution," *Chem. Commun.*, vol. 55, no. 26, pp. 3717–3720, Mar. 2019.
[22] J. G. Lee *et al.*, "A New Family of Perovskite Catalysts for Oxygen-Evolution Reaction in Alkaline Media: BaNiO3 and BaNi0.83O2.5," *J. Am. Chem. Soc.*, vol. 138, no. 10, pp. 3541–3547, Mar. 2016.
[23] L. M. Garten and S. Trolier-Mckinstry, "The field induced e31,f piezoelectric and Rayleigh response in barium strontium titanate thin films," *Appl. Phys. Lett.*, vol. 105, no. 13, 2014.
[24] L. M. Garten *et al.*, "The existence and impact of persistent ferroelectric domains in $MAPbI_3$," *Sci. Adv.*, vol. 5, no. 1, p. eaas9311, Jan. 2019.
[25] L. M. Garten *et al.*, "Relaxor Ferroelectric Behavior in Barium Strontium Titanate," *J. Am. Ceram. Soc.*, vol. 99, no. 5, 2016.
[26] M. E. Holtz *et al.*, "Topological Defects in Hexagonal Manganites: Inner Structure and Emergent Electrostatics," 2017.
[27] R. Fei, W. Li, J. Li, and L. Yang, "Giant piezoelectricity of monolayer group IV monochalcogenides: SnSe, SnS, GeSe, and GeS," *Appl. Phys. Lett.*, vol. 107, no. 17, p. 173104, Oct. 2015.
[28] L. C. Gomes, A. Carvalho, and A. H. Castro Neto, "Enhanced piezoelectricity and modified dielectric screening of two-dimensional group-IV monochalcogenides," *Phys. Rev. B*, vol. 92, no. 21, p. 214103, Dec. 2015.
[29] R. Fei, W. Kang, and L. Yang, "Ferroelectricity and Phase Transitions in Monolayer Group-IV Monochalcogenides," 2016.
[30] H. Yu *et al.*, "Unraveling a novel ferroelectric GeSe phase and its transformation into a topological crystalline insulator under high pressure," *NPG Asia Mater.*, vol. 10, no. 9, pp. 882–887, Sep. 2018.
[31] W. Wu *et al.*, "Piezoelectricity of single-atomic-layer MoS2 for energy conversion and piezotronics," *Nature*, vol. 514, no. 7523, pp. 470–474, Oct. 2014.
[32] X.-W. Shen, Y.-W. Fang, B.-B. Tian, and C.-G. Duan, "Two-dimensional ferroelectric tunnel junction: the case of SnSe."*ACS Appl. Electron. Mater.* 2019, 1, 7, 1133–1140.
[33] M. A. Franzman, C. W. Schlenker, M. E. Thompson, and R. L. Brutchey, "Solution-Phase Synthesis of SnSe Nanocrystals for Use in Solar Cells," *J. Am. Chem. Soc.*, vol. 132, no. 12, pp. 4060–4061, Mar. 2010.
[34] C. Zhang *et al.*, "Two-Dimensional Tin Selenide Nanostructures for Flexible All-Solid-State Supercapacitors," *ACS Nano*, vol. 8, no. 4, pp. 3761–3770, Apr. 2014.
[35] W. Shi *et al.*, "Tin Selenide (SnSe): Growth, Properties, and Applications.," *Adv. Sci. (Weinheim, Baden-Wurttemberg, Ger.*, vol. 5, no. 4, p. 1700602, Apr. 2018.
[36] H. S. Im, Y. R. Lim, Y. J. Cho, J. Park, E. H. Cha, and H. S. Kang, "Germanium and Tin Selenide Nanocrystals for High-Capacity Lithium Ion Batteries: Comparative Phase Conversion of Germanium and Tin," *J. Phys. Chem. C*, vol. 118, no. 38, pp. 21884–21888, Sep. 2014.
[37] L.-D. Zhao *et al.*, "Ultralow thermal conductivity and high thermoelectric figure of merit in SnSe crystals," *Nature*, vol. 508, no. 7496, pp. 373–377, Apr. 2014.
[38] R. Fei, W. Li, J. Li, and L. Yang, "Giant piezoelectricity of monolayer group IV monochalcogenides: SnSe, SnS, GeSe, and GeS," *Appl. Phys. Lett.*, vol. 107, no. 17, p. 173104, Oct. 2015.
[39] J. G. Lee, H. J. Hwang, O. Kwon, O. S. Jeon, J. Jang, and Y. G. Shul, "Synthesis and application of hexagonal perovskite $BaNiO_3$ with quadrivalent nickel under atmospheric and low-temperature conditions," *Chem. Commun.*, vol. 52, no. 71, pp. 10731–10734, 2016.
[40] Y. Takeda, M. Shimada, F. Kanamaru, M. Koizumi, and N. Yamamoto, " PREPARATION AND MAGNETIC PROPERTY OF BaNiO 3 SINGLE CRYSTALS ," *Chem. Lett.*, vol. 3, no. 2, pp. 107–108, Feb. 1974.